

## Numerical Heat Transfer, Part B: Fundamentals



ISSN: 1040-7790 (Print) 1521-0626 (Online) Journal homepage: http://www.tandfonline.com/loi/unhb20

# NEW BOUNDED SKEW CENTRAL DIFFERENCE SCHEME, PART II: APPLICATION TO NATURAL CONVECTION IN AN ECCENTRIC ANNULUS

F. Moukalled & M. Darwish

To cite this article: F. Moukalled & M. Darwish (1997) NEW BOUNDED SKEW CENTRAL DIFFERENCE SCHEME, PART II: APPLICATION TO NATURAL CONVECTION IN AN ECCENTRIC ANNULUS, Numerical Heat Transfer, Part B: Fundamentals, 31:1, 111-133, DOI: 10.1080/10407799708915102

To link to this article: <a href="http://dx.doi.org/10.1080/10407799708915102">http://dx.doi.org/10.1080/10407799708915102</a>

|      | Published online: 19 Apr 2007.             |
|------|--|
|      | Submit your article to this journal 🗷      |
| lılı | Article views: 57                          |
| Q    | View related articles 🗹                    |
| 4    | Citing articles: 10 View citing articles ☑ |

Full Terms & Conditions of access and use can be found at http://www.tandfonline.com/action/journalInformation?journalCode=unhb20

### NEW BOUNDED SKEW CENTRAL DIFFERENCE SCHEME, PART II: APPLICATION TO NATURAL CONVECTION IN AN ECCENTRIC ANNULUS

#### F. Moukalled and M. Darwish

American University of Beirut, Faculty of Engineering & Architecture, Mechanical Engineering Department, P.O. Box 11-0236, Beirut, Lebanon

The bounded skew central difference scheme (NVF SCDS) [1] is used to study numerically the combined effect of vertical  $(\epsilon_x)$  and horizontal  $(\epsilon_x)$  eccentricities on natural convection in an annulus between a heated horizontal cylinder and its square enclosure. Four Rayleigh numbers ( $Ra=10^3$ ,  $10^4$ ,  $10^5$ , and  $10^6$ ), three aspect ratios (R/L=0.1, 0.2, and 0.3), and eccentricity values ranging from -0.3 to 0.3 are considered. At constant enclosure aspect ratio, the total heat transfer increases with increasing Rayleigh number. For constant Rayleigh-number values, convection contribution to total heat transfer decreases with increasing values of R/L. For conduction-dominated flows, heat transfer increases with increasing  $|\epsilon_y|$  and  $|\epsilon_x|$ . For convection-dominated flows, heat transfer increases with decreasing  $|\epsilon_y|$  for  $|\epsilon_y| < 0$ , decreases with increasing  $|\epsilon_y|$  for  $|\epsilon_y| < 0$ , decreases with increasing  $|\epsilon_y|$  for  $|\epsilon_y| < 0$ , and decreases with decreasing  $|\epsilon_x|$  for  $|\epsilon_x| < 0$ . For the case when conduction and convection are of equal importance, there is a critical  $|\epsilon_x|$  for which the total heat transfer is minimum.

#### INTRODUCTION

Several studies dealing with natural-convection heat transfer in enclosures have been reported in recent years because of their relevance to a large number of practical engineering problems. However, most of the numerical and experimental investigations have concentrated on natural convection in isothermal horizontal cylindrical and spherical annuli, with little attention being focused on natural-convection heat transfer in more complex enclosures. In this study, natural convection in the annulus between a heated horizontal circular cylinder placed eccentrically inside a cooled square cylinder is investigated numerically.

Extensive work on natural-convection heat transfer in horizontal cylindrical annuli has been undertaken. Kuehn and Goldstein [2] presented experimental and numerical results for such an annulus, together with an extensive review of the previous research done in the area. Custer and Shaughnessy [3] obtained numerical results for natural convection of liquid metals in a cylindrical annulus. Results for turbulent natural convection using the  $k-\epsilon$  turbulence model were reported by

Received 15 April 1996; accepted 3 July 1996.

Financial support provided by the University Research Board of the American University of Beirut through Grants 48120 and 48122 and computer time granted by R. Moukalled are gratefully acknowledged.

Address correspondence to Professor Fadl Moukalled, Department of Mechanical Engineering, American University of Beirut, P.O. Box 11-0236, Beirut, Lebanon. E-mail: memouk@aub.edu.leb

| NOMENCLATURE      |  |                     |  |  |  |  |  |  |
|-------------------|--|---------------------|--|--|--|--|--|--|
| A<br>P            | surface area for heat transfer specific heat of fluid      | v, V                | dimensional and dimensionless y velocities                   |  |  |  |  |  |
|                   | gravitational acceleration                                 | x, X                | dimensional and dimensionless                                |  |  |  |  |  |
| , <del>Ī</del>    | local and average convection heat<br>transfer coefficients | 17                  | coordinates along the horizontal direction                   |  |  |  |  |  |
| ,                 | thermal conductivity width of cavity                       | <i>y</i> , <i>Y</i> | dimensional and dimensionless coordinates along the vertical |  |  |  |  |  |
| νυ, <del>Νυ</del> | local and average Nusselt numbers                          |                     | direction  |  |  |  |  |  |
| , P               | dimensional and dimensionless                              | α                   | coefficient of thermal diffusivity                           |  |  |  |  |  |
|                   | pressures  | β                   | coefficient of thermal expansion                             |  |  |  |  |  |
| T.                | Prandtl number (= $\mu c_P/k$ )                            | θ                   | dimensionless temperature                                    |  |  |  |  |  |
|                   | total heat transfer from surface                           | ν                   | kinematic viscosity  |  |  |  |  |  |
|                   | radius of inner cylinder                                   | ρ                   | density  |  |  |  |  |  |
| ta                | Rayleigh number $(=g\beta(T_h-T_c)L^3/\nu\alpha)$          | ψ                   | stream function  |  |  |  |  |  |
|                   | arc length   | Subsci              | Subscripts   |  |  |  |  |  |
|                   | distance along the enclosure surface                       |                     |  |  |  |  |  |  |
|                   | dimensional temperature                                    | c                   | cold wall  |  |  |  |  |  |
| , <i>U</i>        | dimensional and dimensionless x                            | h                   | hot wall   |  |  |  |  |  |
|                   | velocities   | max                 | maximum value  |  |  |  |  |  |

Farouk and Guceri [4]. The transient natural-convection behavior was investigated experimentally and numerically by Castrejon and Spalding [5]. The effect of conduction along the walls of a cylindrical annulus on unsteady natural convection was studied by Bubnovich and Kolesnikov [6] and by Kolesnikov and Bubnovich [7]. A comprehensive numerical study of natural convection in horizontal annuli for a wide range of Rayleigh numbers and diameter ratios was performed by Kumar [8]. Recently, Clemes et al. [9] reported on measurements of natural-convection heat transfer in air from isothermal horizontal cylinders of circular and noncircular cross sections at various orientations and for a wide range of Rayleigh number.

A number of workers have also studied natural convection in eccentric cylindrical annuli. The work undertaken by Cho et al. [10] and by Prusa and Yao [11] quantified the effects of eccentricity of the inner cylinder on natural-convection heat transfer. The numerical analysis of Ho and Lin [12] dealt with natural convection of cold water within an eccentric annulus. The flow patterns and heat transfer characteristics were found to be strongly affected by the density inversion of water and the position of the inner cylinder of the annulus. Naylor et al. [13] presented an experimental and numerical study of natural convection between two eccentric tubes.

Sparrow et al. [14] investigated natural convection in enclosures with off-center innerbodies. Lacroix [15] conducted a numerical study of natural convection around two heated horizontal cylinders inside a rectangular cavity cooled from above. A study reported by Ho et al. [16] dealt with natural convection between two horizontal cylinders (one heated and one cooled) in an adiabatic circular enclosure.

Natural-convection heat transfer from a square cylinder placed in a cylindrical enclosure was reported by Chang et al. [17]. More recently, Oosthuizen and Paul [18] studied natural convection from a prismatic cylinder in a square enclo-

sure. Experimental studies of natural convection between concentrically mounted bodies (spheres, cylinders, and cubes) and their spherical and cubical enclosures were undertaken by Warrington and Powe [19] at moderate Rayleigh numbers and by Warrington et al. [20] at low Rayleigh numbers. In both studies, correlations between Nusselt number and Rayleigh number were presented and the effect of the enclosure shape was seen to be small so long as the appropriate length scale was employed. Ghaddar [21] investigated natural convection around a cylindrical rod placed in an enclosure with a hydraulic diameter that is nearly 40 times the cylinder diameter. The study of Moukalled and Acharya [22] was for a similar geometry with a dimensionless gap width in the range of 3 to 10 and for a uniform-temperature boundary condition. This work was then extended [23] to the situation where the inner heated circular cylinder is vertically eccentric.

In most of the work mentioned above, an upwind or upwindlike scheme for the calculation of the convective flux was used. This class of schemes, however, is known and was shown in a companion article [1] to be highly diffusive in both the cross-stream and streamwide directions. In order to minimize numerical errors and to exploit the high accuracy of the NVF SCDS in recirculating flows (as was shown in [1]), this scheme is adopted in this article to extend the work reported by Moukalled and Acharya [22, 23] into situations where the inner cylinder is eccentric in both the horizontal and vertical directions (Figure 1a) and to study numerically the details of natural-convection heat transfer of air in the annulus.

#### **GOVERNING EQUATIONS**

The physical situation under consideration is depicted in Figure 1a. The equations governing the flow and temperature fields are those that express the conservation of mass, momentum, and energy. The flow, driven by buoyant forces, is assumed to be steady, laminar, and two-dimensional. The Boussinesq approximation is used to incorporate the temperature dependence of density in the conservation equations. Further, density fluctuations in the fluid are assumed to be sufficiently small that they need only be included in the body-force term of the y-momentum equation. With these assumptions, the nondimensional mass, momentum, and energy equations become

$$\frac{\partial U}{\partial X} + \frac{\partial V}{\partial Y} = 0 \tag{1}$$

$$U\frac{\partial U}{\partial X} + V\frac{\partial U}{\partial Y} = -\frac{\partial P}{\partial X} + \frac{\partial^2 U}{\partial X^2} + \frac{\partial^2 U}{\partial Y^2}$$
 (2)

$$U\frac{\partial V}{\partial X} + V\frac{\partial V}{\partial Y} = -\frac{\partial P}{\partial Y} + \frac{\partial^2 V}{\partial X^2} + \frac{\partial^2 V}{\partial Y^2} + \frac{\operatorname{Ra}\theta}{\operatorname{Pr}}$$
(3)

$$U\frac{\partial\theta}{\partial X} + V\frac{\partial\theta}{\partial Y} = \frac{1}{\Pr}\left(\frac{\partial^2\theta}{\partial X^2} + \frac{\partial^2\theta}{\partial Y^2}\right) \tag{4}$$

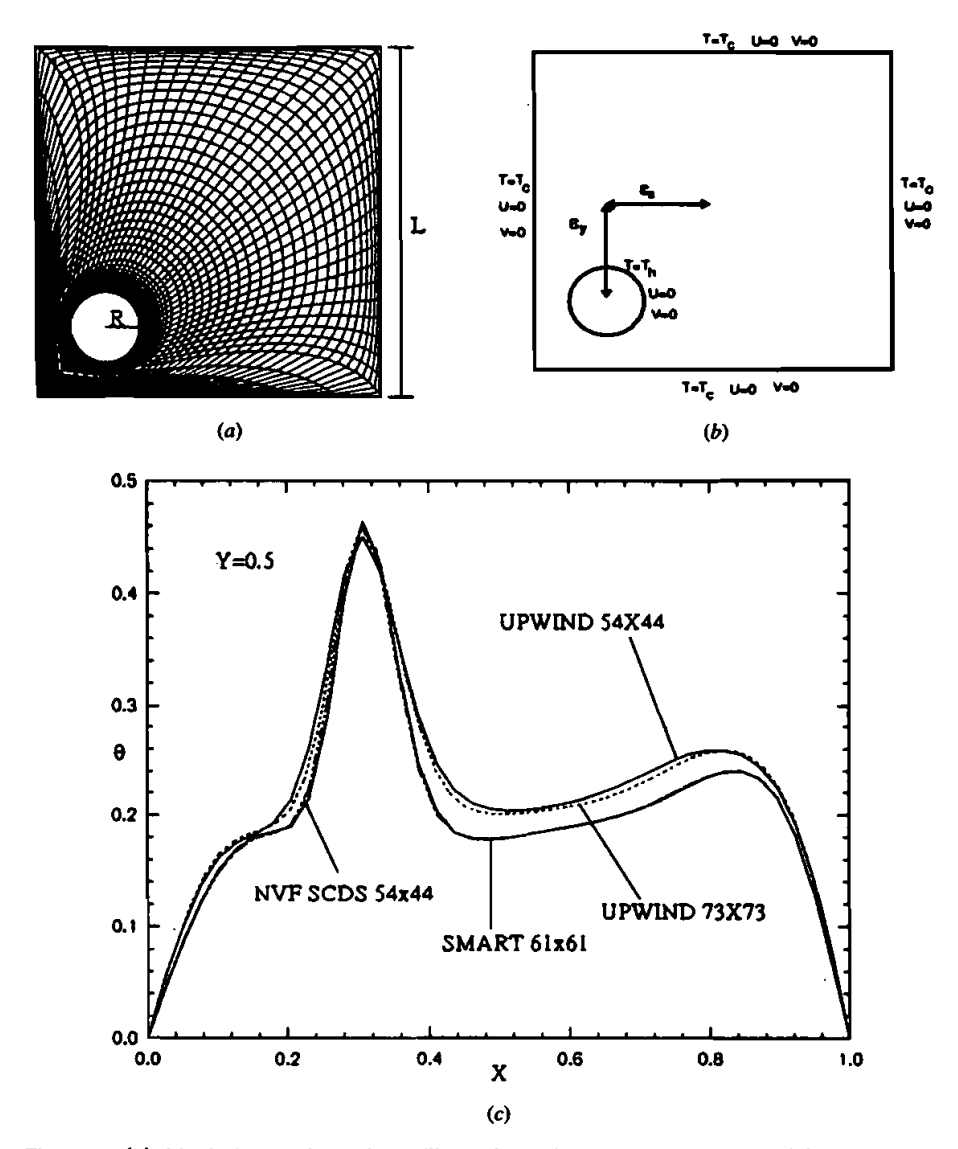


Figure 1. (a) Physical domain and an illustrative grid network generated. (b) Horizontal eccentricity, vertical eccentricity, and boundary conditions. (c) Comparison of temperature profiles along the horizontal centerline of the domain, generated using different schemes and grid densities.

where the following dimensionless variables have been used:

$$X = \frac{x}{L} \qquad Y = \frac{y}{L} \tag{5}$$

$$U = \frac{u}{\nu/L} \qquad V = \frac{v}{\nu/L} \tag{6}$$

$$P = \frac{p + \rho g y}{\rho(\nu/L)^2} \qquad \theta = \frac{T - T_c}{T_h - T_c} \tag{7}$$

To close the system of equations, hydrodynamic and thermal boundary conditions are needed. Along the walls of the enclosure the velocity components are set to zero, while, the nondimensional uniform temperatures of 1 and 0 are maintained along the hot and cold walls, respectively (Figure 1b).

#### SOLUTION PROCEDURE AND COMPUTATIONAL DETAILS

The conservation equations [Eqs. (1)-(4)] are transformed into curvilinear coordinates and solved numerically using the control-volume approach. The details of the method are described in a companion article [1] and are not repeated here. This includes the use of the new NVF SCDS and the treatment of the nonorthogonal terms in the pressure correction equation suggested by Cho and Chung [24]. An additional and important issue to be considered here is the discretization of the computational domain. Grid points should be distributed in such a way as to resolve accurately the physics involved. Therefore, denser clustering is needed near walls, where hydraulic and thermal boundary layers develop. For that purpose, the method of Thomas and Middlecoff [25] is used. This method generates grids by solving a system of Poisson equations and allows the grid-point distribution in the interior of the domain to be controlled directly by the selection of the grid-point distribution along the boundaries. An illustrative grid network generated is depicted in Figure 1a.

Furthermore, since the transformation from the physical domain into the computational domain involves a branch cut, the boundary conditions are not known explicitly at the common interface. In order to incorporate their values smoothly, the cyclic tridiagonal matrix algorithm [26] is used when solving the system of equations in the  $\xi$  direction, while the normal tridiagonal matrix algorithm is employed in the  $\eta$  direction.

The results presented next are computed using  $54 \times 44$  unevenly distributed grid points. This grid is found to be more than sufficient to produce grid-independent results. Comparison of the solution on a  $54 \times 44$  grid (2,376 grid points) with the solution on a  $75 \times 54$  grid (3,996 grid points) revealed that the maximum differences were less than 0.22% in the peak Nusselt number value and less than 0.16% in the peak mid-height horizontal velocity. Conservation of mass, momentum, and energy was found to be satisfied to within 0.0001% in each control volume. Comparison was also made with results obtained using the upwind and SMART schemes and is displayed in Figure 1c. From this figure it can be inferred that results generated by SMART on a denser grid ( $62 \times 62$ ) are similar to those generated by the NVF SCDS on a grid of size  $54 \times 44$ , which is an indication of

the high accuracy of the scheme used. On the other hand, results obtained by the upwind scheme are very diffusive even on a much denser grid of size  $73 \times 73$ .

#### **RESULTS AND DISCUSSION**

The main parameters of interest in this study are the enclosure aspect ratio (R/L), the Rayleigh number Ra, the Prandtl number Pr, and the eccentricities in the horizontal,  $\epsilon_x$ , and vertical,  $\epsilon_y$ , directions. Vertical/horizontal eccentricity is defined as the dimensionless vertical/horizontal distance between the centers of the inner circular and outer square cylinders and is taken to be positive for upward/right displacement of the inner cylinder. Parameter values considered are three different aspect ratios  $(R/L=0.1,\ 0.2,\ \text{and}\ 0.3)$ , four Rayleigh number values  $(Ra=10^3,\ 10^4,\ 10^5,\ \text{and}\ 10^6)$ , and eccentricity values ranging from -0.3 to 0.3. Air is considered to be the working fluid, and the Prandtl number is fixed at 0.71.

The results are presented in the form of representative streamlines and isotherms, mid-height and mid-width velocity and temperature profiles, and local and average Nusselt number values.

#### Streamlines and Isotherms

The influence of Rayleigh number and eccentricity on the flow and temperature fields is revealed by the streamline and isotherm plots depicted in Figures 2-5. Figures 2 and 3 show the effect of Rayleigh number on natural convection for given values of the horizontal and vertical eccentricities. Figures 4 and 5 reveal the effect of eccentricity on heat transfer at a given Rayleigh number.

The effects of Rayleigh number on heat transfer for negative eccentricities of the inner cylinder are depicted in Figure 2. As shown, the main flow consists of two recirculating eddies, with the one in the wide gap region rotating clockwise and the left vortex rotating counterclockwise. This indicates that air is moving up along the heated inner cylinder and down along the vertical cold sides of the enclosure. At low Ra (Ra = 10<sup>3</sup>, not shown for compactness), the eye of the left rotating eddy is close to the hot wall; as Ra increases, however, the eye moves upward toward the upper cold wall of the enclosure. This phenomenon is more pronounced at lower R/L values (R/L = 0.1) because of the larger available convective area above the inner circular cylinder. Moreover, the center of the right vortex, located close to the center of the domain at low Ra, also moves upward as Ra is increased, and at the highest Rayleigh number presented, this recirculating eddy exhibits two vortex cores, which rotate in the clockwise direction (Figures 2a-2d.). Furthermore, at the higher aspect ratio (R/L = 0.2), the flow separates and forms a weak vortex below the left-hand portion of the inner cylinder because of higher viscous effects in combination with higher stratification levels.

As mentioned above, at low values of Ra the convective flow is weak (Figures 2a and 2c), and isotherms (Figures 2e and 2g) indicate a conductionlike behavior,

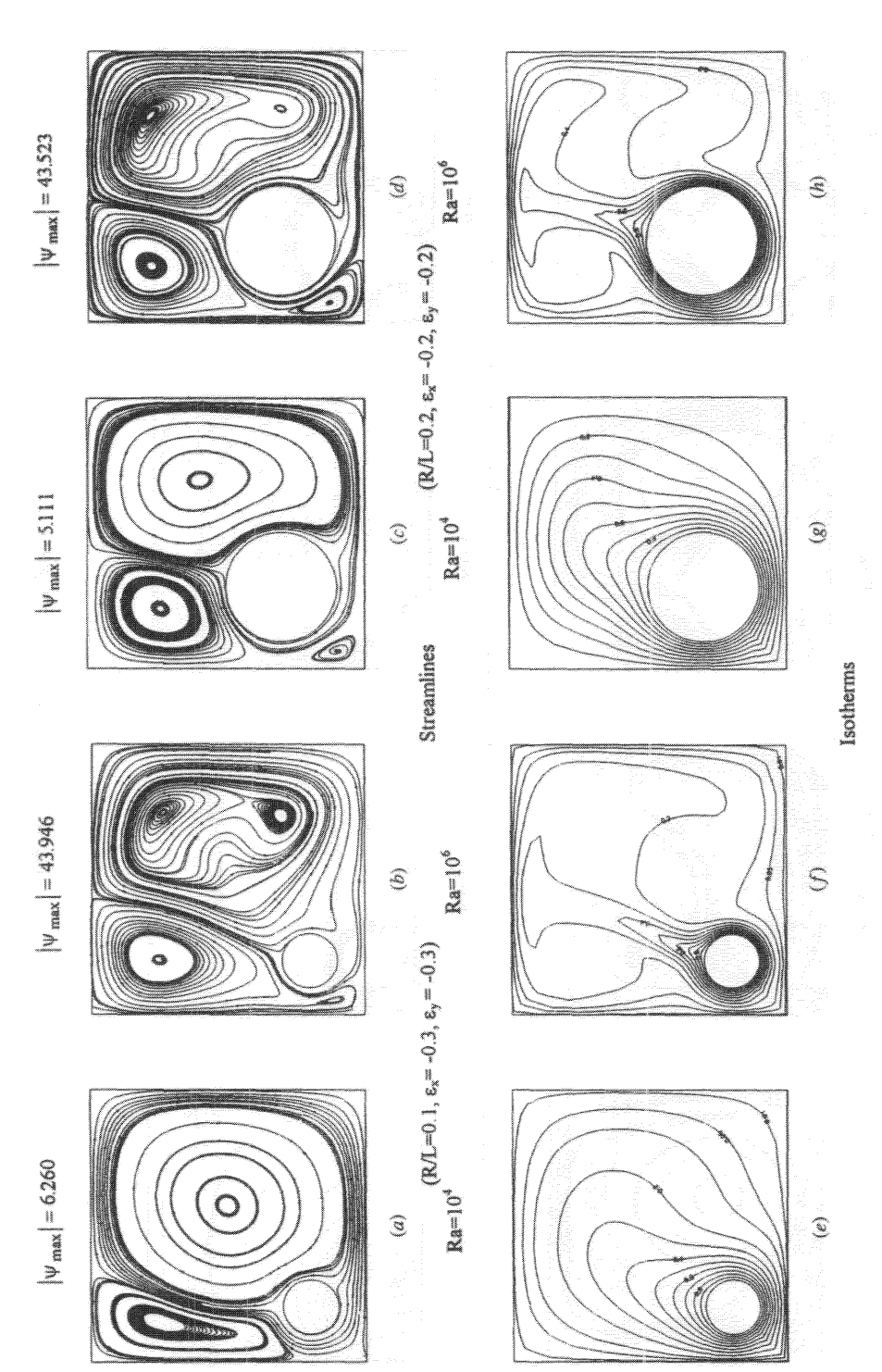


Figure 2. Streamline and isotherm plots.

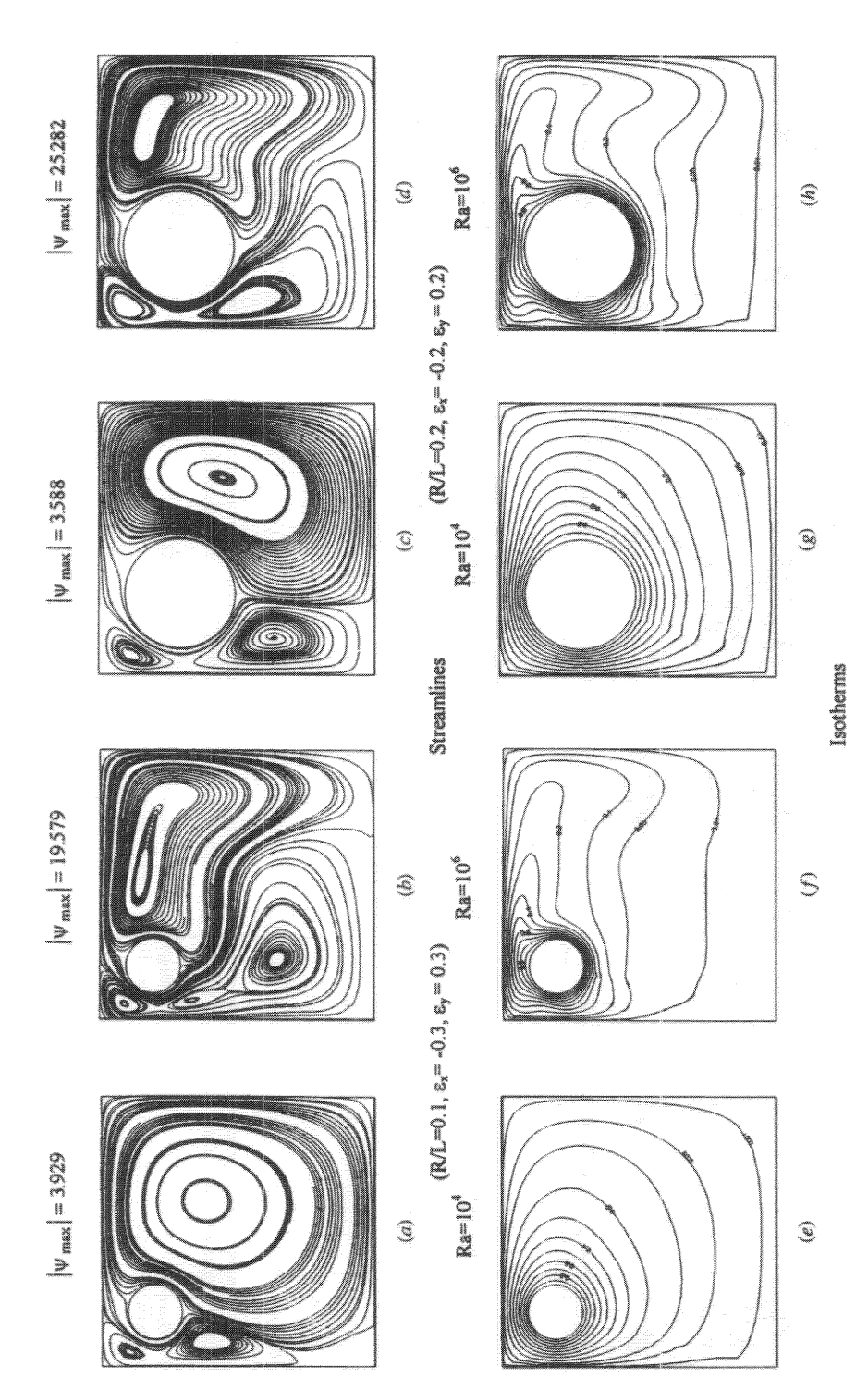


Figure 3. Streamline and isotherm plots.

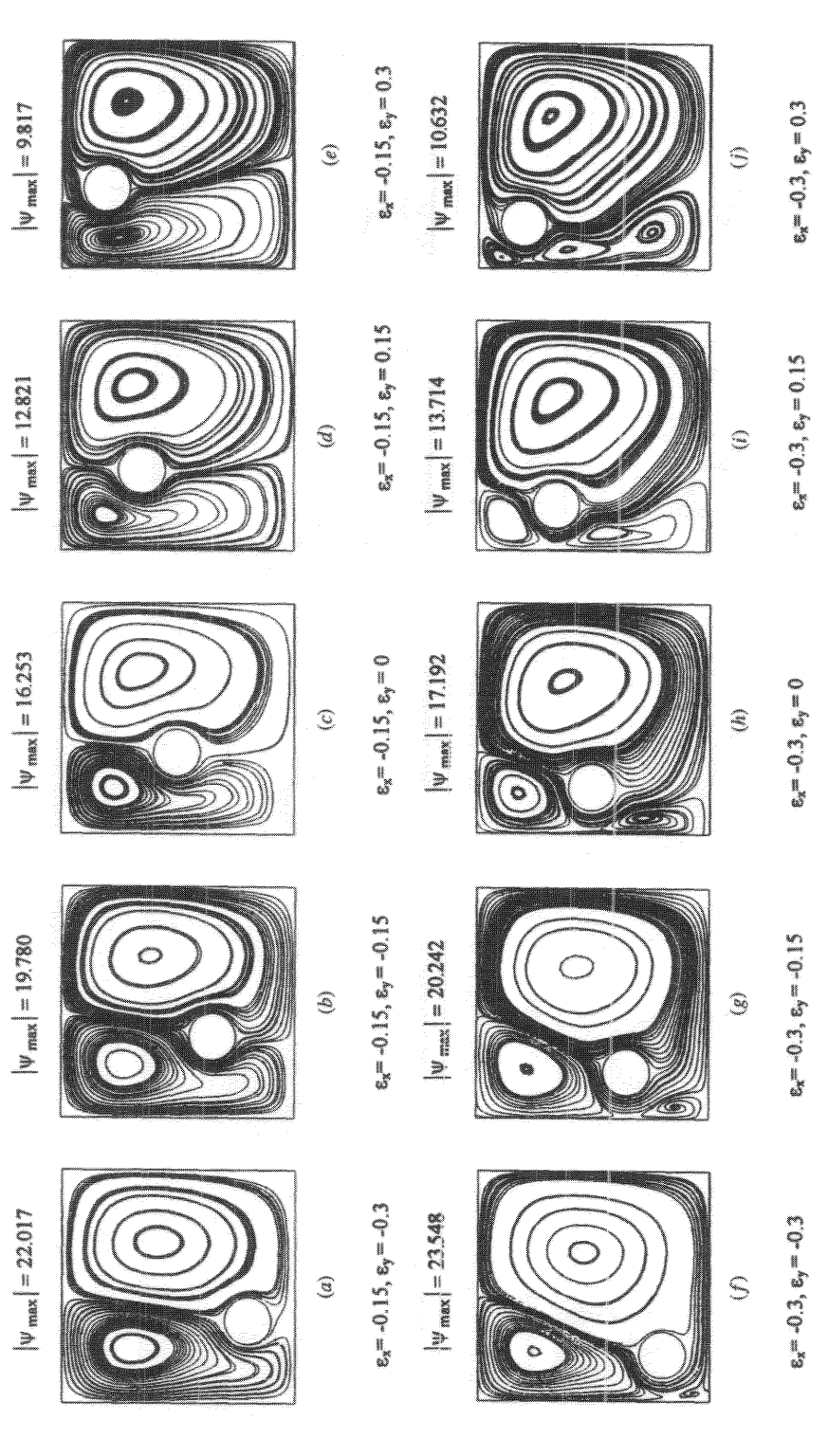


Figure 4. Streamline plots  $(R/L = 0.1, Ra = 10^5)$ .

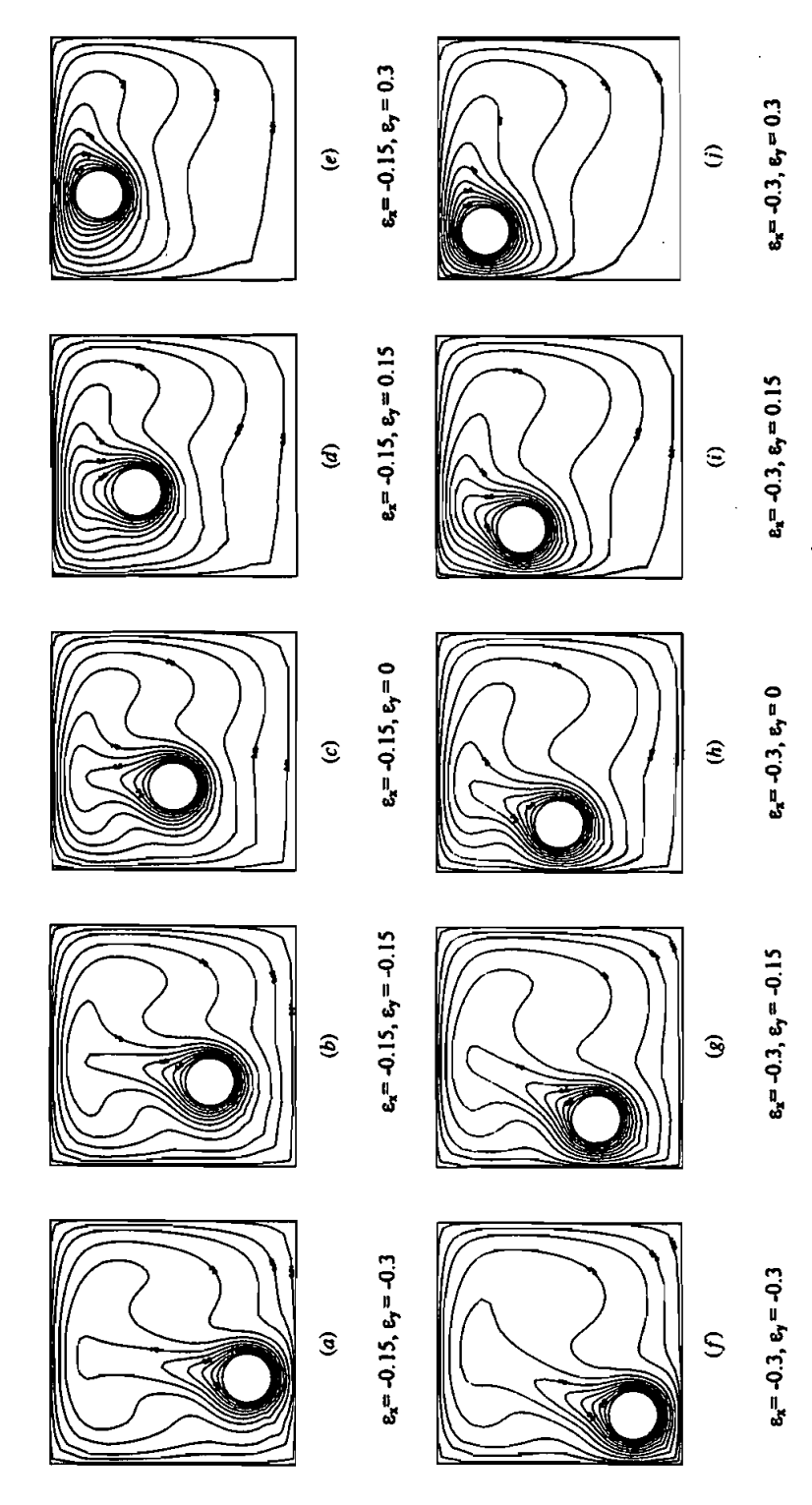


Figure 5. Isotherm plots  $(R/L = 0.1, Ra = 10^5)$ .

and flow-induced stratification effects are very small. As Ra is increased from 10<sup>3</sup> to 106, the convective flow strength increases. However, because of the small convective area below the inner cylinder, flow-induced stratification effects remain small. As shown, flow-induced thermal stratification in the primary flow area above the inner cylinder does not occur, and the effect of moving the inner cylinder downward is to increase the primary flow area or the effective length scale, thus increasing the convective flow strength above the inner cylinder. Moreover, at high Ra, the convective flow strength being significant, isotherm plots (Figures 2f and 2h) clearly show the boundary-layer behavior on the lower part of the heated cylinder and the upper part of the cooled enclosure. The boundary layer along the inner cylinder separates near the top of the cylinder, and forms a thermal plume. One can easily notice that the plume is not rising vertically above the inner tube. Rather, because of a stronger recirculating vortex in the wide gap region, the plume is shifted off the top of the inner cylinder. Moreover, the phenomenon of temperature inversion, which indicates that fluid in the region close to the hot inner circular cylinder is cooler than that close to the outer square cylinder, is observed at high Rayleigh numbers (see Figures 2f and 2h). The extent of temperature inversion is seen to be much higher for lower R/L values as a result of enhanced natural convection at lower R/L values.

Figure 3 reveals the influence of buoyancy forces on heat transfer for positive vertical eccentricities (that is,  $\epsilon_y > 0$  and  $\epsilon_x < 0$ ). At low Ra, the flow patterns and isotherms are qualitatively similar to those for negative eccentricities. The strength of convection is higher at higher Ra values. In contrast with negative eccentricities, flow-induced thermal stratification effects become increasingly important at high Ra, and in view of the fact that the cooled outer surface is proportionately larger than the heated inner surface, stratification effects are primarily significant below the horizontal diameter of the inner cylinder. Therefore, for positive  $\epsilon_y$ , where a greater proportion of the flow area is in the bottom half, stratification effects are significantly more important than for the case with negative  $\epsilon_y$ .

The weak recirculation bubble increases in size with increasing values of Ra. This is caused by stratification, which makes it difficult for the flow descending the cooled wall to penetrate the lower region. Moreover, the core of the strong clockwise-rotating vortex moves upward. Because of the relatively narrow gap near the top of the enclosure, no evidence of plume development is found above the heated inner cylinder (see Figures 3e-3h). Instead, near the top of the heated cylinder, a local region of conduction-dominated heat transfer is produced, a phenomenon that is usually found at the bottom portion of the annulus where the flow is inert and stably stratified. Isotherm plots indicate a weak distortion even at high Rayleigh-number values. The  $|\psi_{max}|$  values presented in Figures 2 and 3 indicate that the flow strength increases with increasing Ra and/or the convective area above the inner cylinder.

The effects of eccentricity on the flow and temperature fields can be inferred from the maximum stream function estimates and the streamline and isotherm plots presented in Figures 4 and 5, respectively. At a given horizontal eccentricity, as the inner cylinder is moved upward (Figure 4), flow-induced thermal stratification below the cylinder increases, leading to a reduction in the flow strength. This

is clearly seen from the  $|\psi_{\text{max}}|$  values shown in Figure 4. Moreover, the increase in thermal stratification below the inner cylinder as it is moved upward is evident in the isotherm patterns shown in Figure 5.

At a given vertical location of the inner cylinder, increasing  $|\epsilon_x|$  results in an increase in the flow strength in the wide gap region due to a higher convective area as revealed by the  $|\psi_{\text{max}}|$  values presented in Figure 4 and the higher distortion of isotherms depicted in Figure 5. However, this increase in flow strength in the right portion of the domain is associated with a reduction in the available convective area in the left portion and a splitting of the left vortex into two. This reduces the left contribution to heat transfer and may lead to a reduction in total heat transfer, as discussed later.

Finally, streamline plots for R/L=0.3, not presented here for compactness, did not reveal any separation of the flow above the cylinder for all cases considered in this work. This is in contrast with results displayed in [22, 23] for the case when  $\epsilon_x=0$ . In order to eliminate any doubt about the computations, the concentric case for R/L=0.3 and  $Ra=10^5$ , a case for which separation was predicted in [22], was solved, over the whole physical domain and not half of it, using the numerical techniques presented in this work. The results generated were in accordance with those reported in [22] and revealed separation at the top of the cylinder. The difference in Nusselt-number values between the two results was less than 0.04% (this slight difference, even though a high-solution scheme is used, is due to low convection effects at high R/L values). The disappearance of separation is attributed to enhanced convection effects as  $\epsilon_x$  increases.

#### **Velocity and Temperature Profiles**

The temperature profiles along the horizontal and vertical centerlines are shown in Figure 6, for R/L=0.1 and  $\epsilon_x=-0.3$ . The plots depicted in Figure 6a reveal that for a negative vertical eccentricity ( $\epsilon_y=-0.3$ ), the temperature profiles along the horizontal centerline are steeper near the left vertical wall of the domain at higher Ra because of stronger convection effects. Moreover, the maximum temperatures at all Ra values are seen to occur in the thermal plume region above the inner hot cylinder, as expected. Furthermore, the phenomenon of temperature inversion is clearly evident from the profiles at Ra =  $10^5$  and  $10^6$ . For a positive vertical eccentricity (Figure 6b,  $\epsilon_y=0.3$ ), the level of temperature decreases as Ra increases, because of higher stratification effects below the hot cylinder, which in this case is above the horizontal centerline of the enclosure.

Along the vertical centerline and for  $\epsilon_y = -0.3$  (Figure 6c), the maximum temperature, close to the bottom wall at Ra =  $10^3$ , moves upward toward the top wall as Ra increases, because of higher stratification effects in the lower part of the domain and stronger convective motion in the upper portion. This is associated with a decrease in the temperature gradient in the vicinity of the bottom wall and an increase near the top wall. The peak in the profiles for  $\epsilon_y = 0.3$  (Figure 6d) is similar but less pronounced, because of the fact that the hot cylinder is near the top wall of the enclosure.

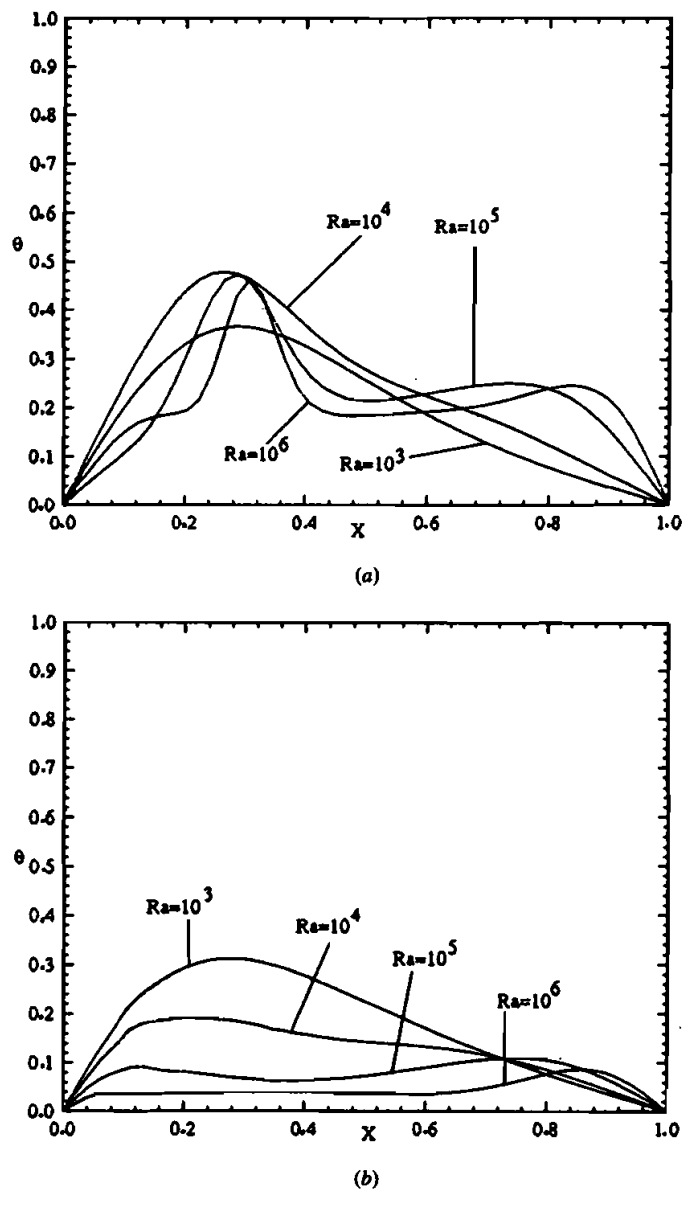


Figure 6. Temperature profiles at: (a) Y = 0.5 (R/L = 0.1,  $\epsilon_x = -0.3$ ,  $\epsilon_y = -0.3$ ); (b) Y = 0.5 (R/L = 0.1,  $\epsilon_x = -0.3$ ,  $\epsilon_y = 0.3$ ).

The vertical and horizontal velocity components along the horizontal and vertical centerlines of the domain are displayed in Figure 7 for R/L=0.1 and  $\epsilon_x=-0.3$ . These velocity components are very small at Ra =  $10^3$ , indicating negligible convection effects and a weak flow field. Moreover, as Ra increases, their magnitude increases, indicating an increase in the flow strength. Further-

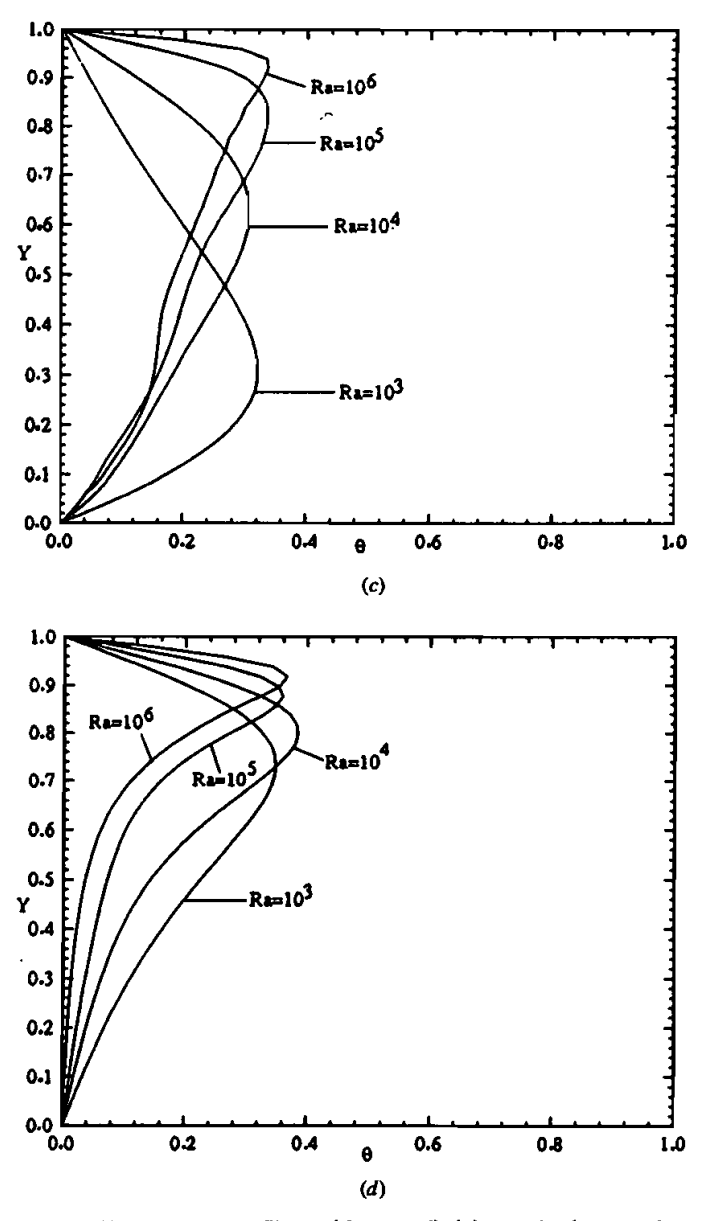


Figure 6. Temperature profiles at (Continued): (c) X = 0.5 (R/L = 0.1,  $\epsilon_x = -0.3$ ,  $\epsilon_y = -0.3$ ); (d) X = 0.5 (R/L = 0.1,  $\epsilon_x = -0.3$ ,  $\epsilon_y = 0.3$ ).

more, the boundary-layer behavior in the vicinity of the walls is evident and the velocity gradient there increases with Ra.

The vertical velocity component along the horizontal centerline for a negative vertical eccentricity (Figure 7a) reveals the upward flow motion above the hot inner cylinder and the descending flow motion near the left and right walls of the

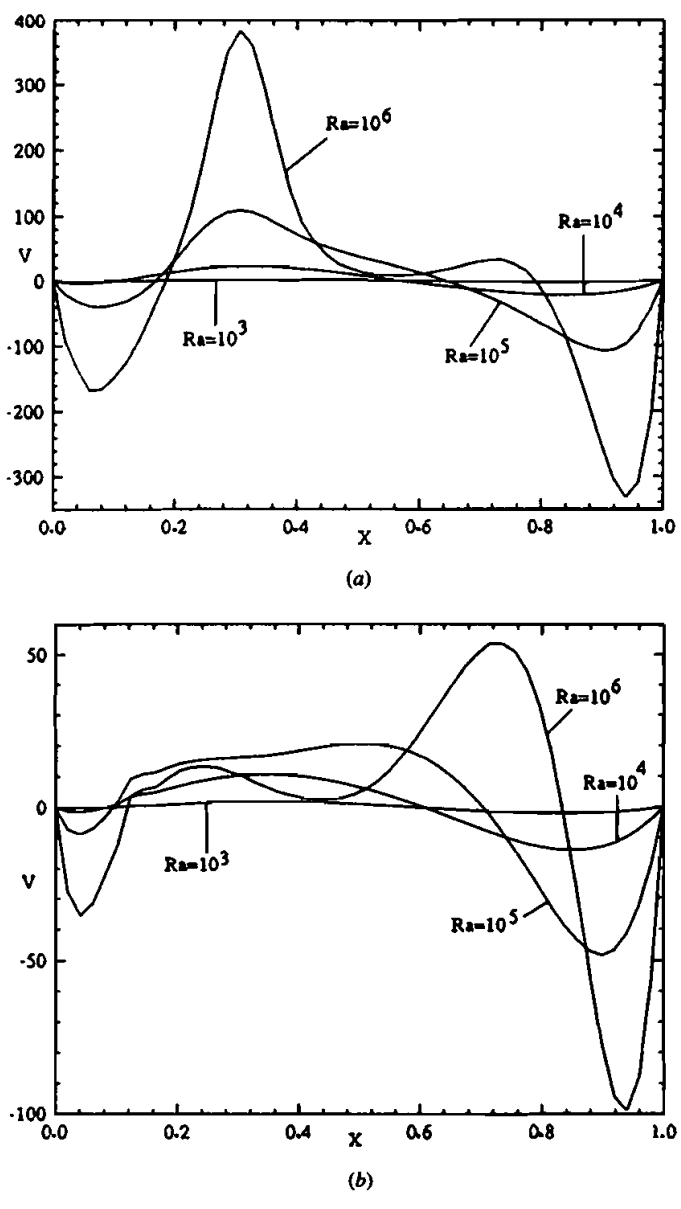


Figure 7. V-velocity profiles at: (a) Y=0.5 (R/L=0.1,  $\epsilon_x=-0.3$ ,  $\epsilon_y=-0.3$ ); (b) Y=0.5 (R/L=0.1,  $\epsilon_x=-0.3$ ,  $\epsilon_y=0.3$ ).

enclosure, which is in accordance with the streamline plots presented earlier. For a positive vertical eccentricity (Figure 7b), the magnitude of the V-velocity component is seen to be much lower, especially in the left portion of the domain below the hot inner cylinder, where the flow is thermally stratified. The U-velocity

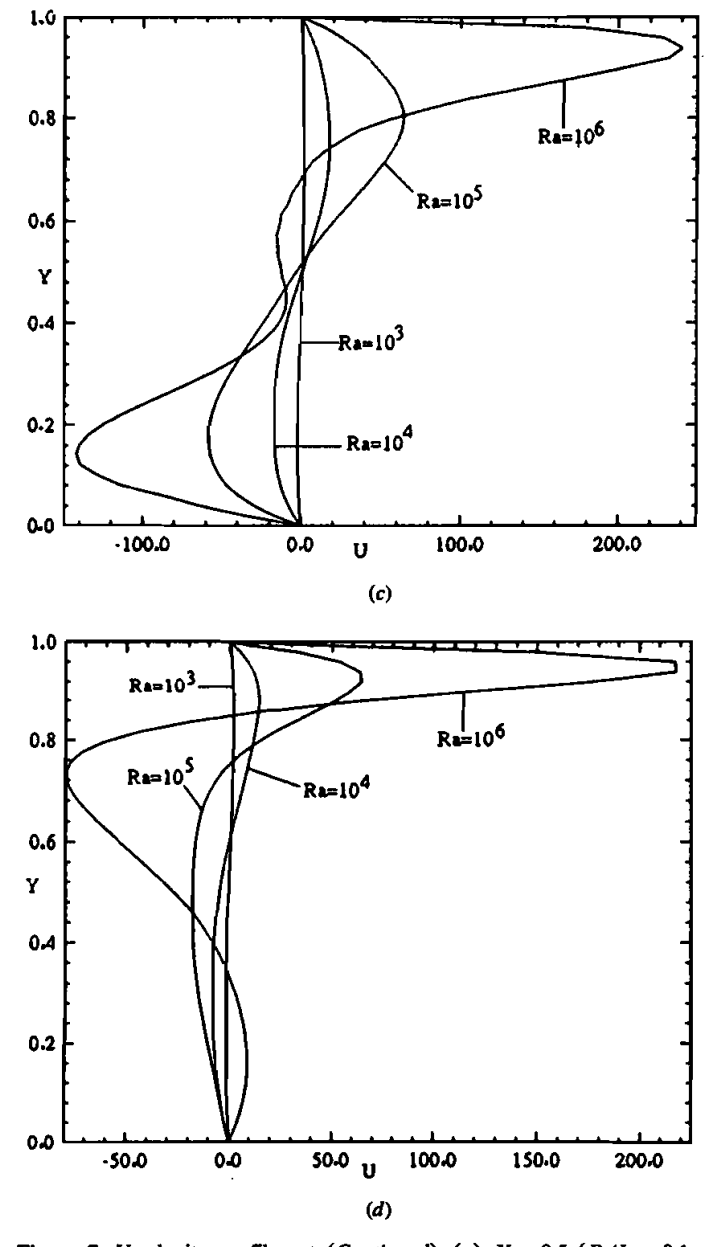


Figure 7. U-velocity profiles at (Continued): (c) X = 0.5 (R/L = 0.1,  $\epsilon_x = -0.3$ ,  $\epsilon_y = -0.3$ ); (d) X = 0.5 (R/L = 0.1,  $\epsilon_x = -0.3$ ,  $\epsilon_y = 0.3$ )

profiles along the vertical centerline are depicted in Figure 7c for a negative vertical eccentricity and in Figure 7d for a positive one. As shown, for  $\epsilon_y < 0$ , thermal stratification is not important and the velocity is high in the lower and upper parts of the domain. For  $\epsilon_y > 0$ , however, thermal stratification is important in the lower part of the enclosure, where the velocity is seen to be very small.

#### **Nusselt Numbers**

The local heat transfer coefficient and Nusselt number along the hot and cold walls are computed using the following definitions:

$$h_h = -\frac{k[\partial T/\partial n]_h}{[T_h - T_c]} \qquad h_c = -\frac{k[\partial T/\partial n]_c}{[T_h - T_c]}$$
(8)

$$Nu_h = \frac{h_h S_{h, \text{max}}}{k} \qquad Nu_c = \frac{h_c S_{c, \text{max}}}{k}$$
 (9)

where n denotes the normal distance from the wall and S the distance along the wall measured from its lowest point for the hot inner cylinder and from the lower left corner for the cold, square enclosure. The average heat transfer coefficients and Nusselt numbers are calculated as

$$\overline{h_h} = -\frac{Q_{\text{conv}}}{A_h(T_h - T_c)} \qquad \overline{h_c} = -\frac{Q_{\text{conv}}}{A_c(T_h - T_c)}$$
 (10)

$$\overline{Nu_h} = \frac{\overline{h_h} S_{h, \max}}{k} \qquad \overline{Nu_c} = \frac{\overline{h_c} S_{c, \max}}{k}$$
 (11)

where  $Q_{\text{conv}}$  is the overall convection heat transfer and  $A_h$  and  $A_c$  are the heat transfer areas along the hot and cold walls, respectively. Since  $\overline{h_h}S_{h, \max} = \overline{h_c}S_{c, \max}$ , it follows that  $\overline{\text{Nu}_h} = \overline{\text{Nu}_c} = \overline{\text{Nu}}$ .

The normalized local Nusselt number distributions  $Nu^*$  ( $Nu^* = Nu/Nu_0$ , where  $Nu_0$  is the value of Nusselt number for pure conduction, that is, Ra = 0) along the hot and cold walls are presented in Figure 8, for positive and negative vertical eccentricities of the inner cylinder. In this normalized form, the relative effect of convection can be assessed directly. Values are plotted as a function of  $S/S_{max}$ , where  $S_{max}$  is the maximum possible value of S.

The profiles presented show that, at low Ra, conduction is the dominant heat transfer mode in the whole enclosure (Nu\*  $\approx$  1) for both positive and negative eccentricities of the inner cylinder. At high Ra, convection contribution to total heat transfer is shown to be important, with its magnitude being dependent on the eccentricity of the inner cylinder. The variations in Nu\* along the hot and cold walls are presented in Figures 8a and 8b for  $\epsilon_y < 0$ . Over the hot wall, Nu\* increases along the right lower quarter of the cylinder and decreases along the right upper quarter. The peak close to the right end of the horizontal diameter  $(S_h/S_{h, \max} \approx 0.25)$  is due to the rising cold fluid impinging on the hot cylinder, as revealed by the streamlines presented in Figure 2. As expected, minimum heat transfer occurs close to the highest point on the cylinder  $(S_h/S_{h, \max} \approx 0.5)$ , where the two streams rising around its left and right faces separate to form a thermal plume. The left face contribution  $(0.5 \le S_h/S_{h, \max} \le 1)$  to convection heat transfer is much lower than the right face contribution because of weaker flow strength

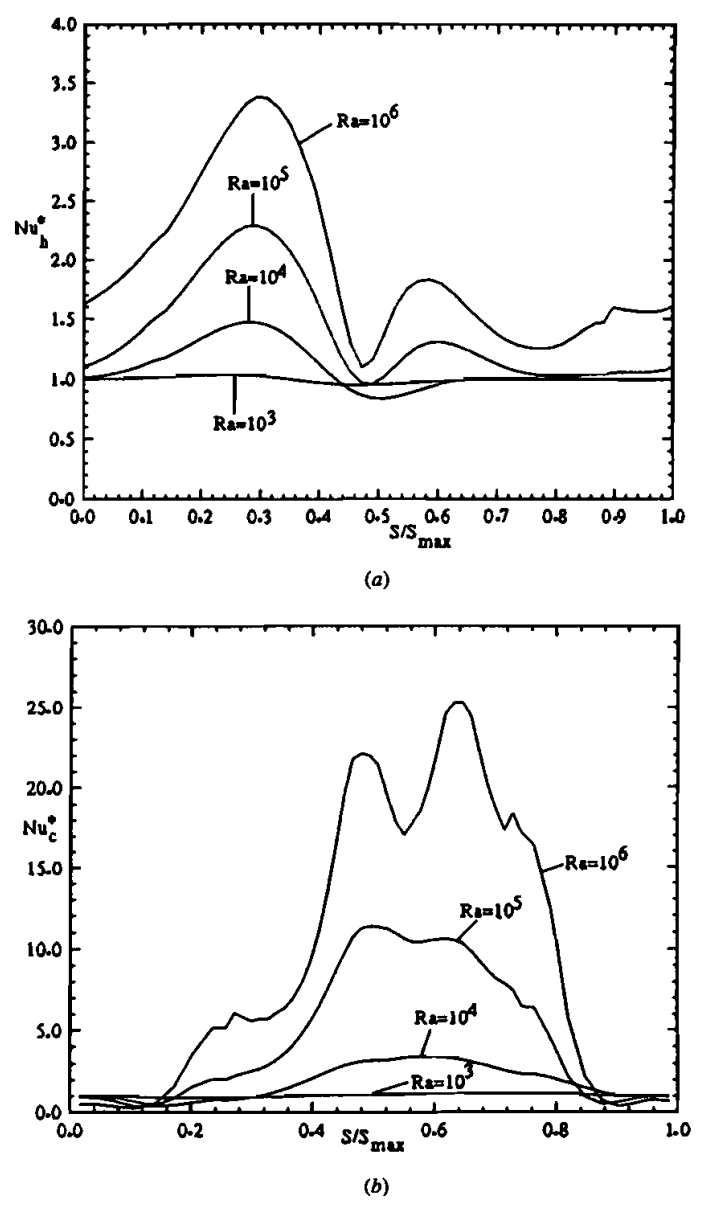


Figure 8. Nusselt-number distribution along: (a) the hot wall  $(R/L=0.1,\ \epsilon_x=-0.3,\ \epsilon_y=-0.3)$ ; (b) the cold wall  $(R/L=0.1,\ \epsilon_x=-0.3,\ \epsilon_y=-0.3)$ .

caused by lower available convective area. A second minimum in convection occurs at the left end of the horizontal diameter  $(S_h/S_{h,\,\rm max}\approx 0.75)$ , where the convective area is minimum. A second peak (of lower value) is observed over the left upper quarter of the cylinder  $(0.5\leqslant S_h/S_{h,\,\rm max}\leqslant 0.75)$  and is due to the two counteracting effects of increase in fluid temperature and flow strength. The decrease in

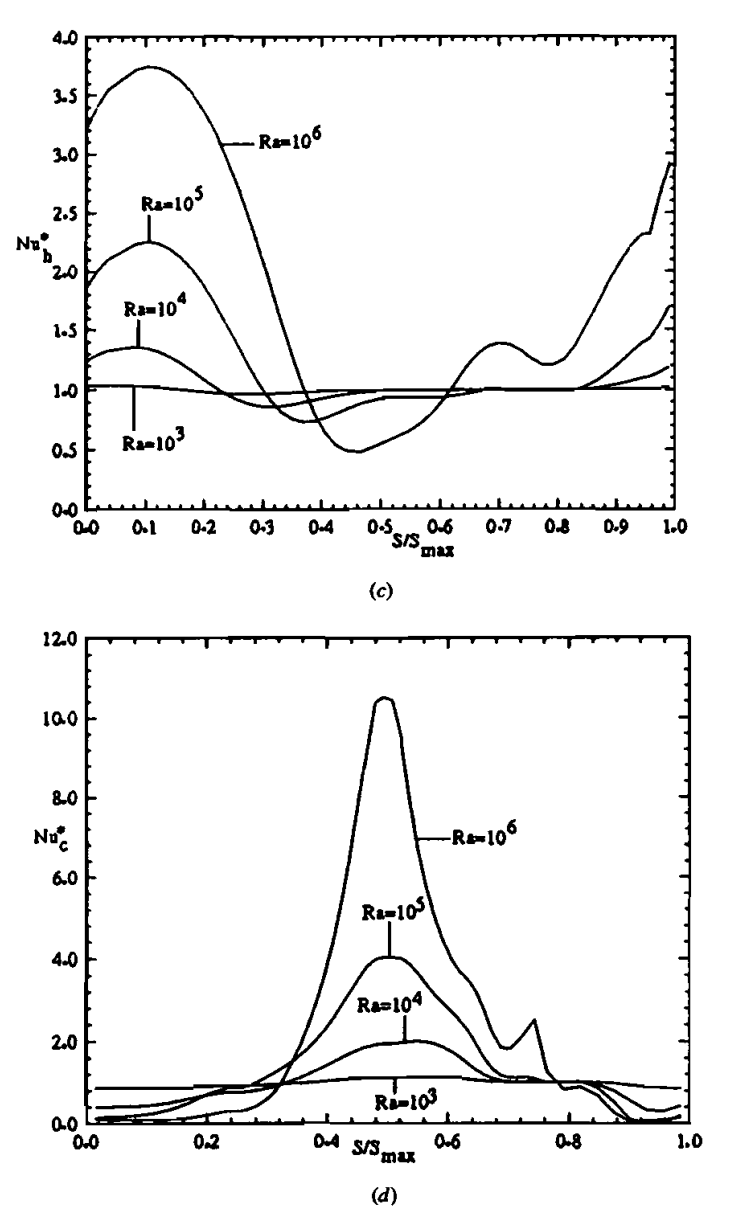


Figure 8. Nusselt-number distribution along (*Continued*): (c) the hot wall  $(R/L=0.1, \epsilon_x=-0.3, \epsilon_y=0.3)$ ; (d) the cold wall  $(R/L=0.1, \epsilon_x=-0.3, \epsilon_y=0.3)$ .

convection over the lower left quarter  $(0.75 \le S_h/S_{h,\,\rm max} \le 1)$  as the fluid rises is due to the increase in fluid temperature and decrease in the flow strength.

The normalized Nusselt-number distribution along the cold wall (Figure 8b) shows that, at relatively high Ra, convection is most important over the top and right walls of the enclosure. Along the lower portion of the right wall and the left

portion of the bottom wall, where the flow is weak, conduction is the dominant heat transfer mode (Nu\* < 1). A maximum is observed in the upper region and is due to the hot fluid from the inner wall rising upward and impinging on the cold top wall, thereby increasing convection heat transfer. Heat transfer then decreases as the fluid moves on the top wall in both directions (left and right). The second peak in Nu\* along the upper part of the right cold wall is due to the tendency of the relatively hot fluid to be deflected away from the upper right corner of the domain (where a local minimum in convection heat transfer occurs) and to encroach upon the right cold wall of the enclosure.

For a positive vertical eccentricity, convection heat transfer is important over the lower portion of the hot inner cylinder (Figure 8c). Maximum convection heat transfer occurs at the location where the cold fluid from the lower right part of the enclosure, not being able to penetrate the lower left part of the domain because of high thermal stratification, rises and impinges on the lower right quarter of the cylinder. Then, this fluid splits into two streams which move around the cylinder in opposite directions. As the two streams progress, they become hotter and convection heat transfer decreases. Along the upper portion of the hot cylinder, conduction is the dominant heat transfer mode, as revealed by the values of  $Nu^*$  ( $Nu^* < 1$ ) and the isotherm plots in Figure 3. The  $Nu^*$  distribution over the cold wall (Figure 8d) shows an increase in convection heat transfer on the right and top walls of the enclosure. Convection effects are seen to maximize near the right upper corner of the outer square cylinder because of low conduction heat transfer at Ra = 0. Along the lower and left walls, where the flow is stratified, heat transfer is governed by conduction ( $Nu^* < 1$ ).

The average Nusselt-number values for all cases studied are given in Table 1. For comparison purposes, the Nu values presented by Moukalled and Acharya [22, 23] for  $\epsilon_r = 0$  are also included in the table. At Ra values of  $10^3$  and  $10^4$ , the overall heat transfer appears to be strongly dominated by conduction. Convection contribution to heat transfer is important at Rayleigh number values of 10<sup>5</sup> and  $10^6$ . This seems to be true for R/L = 0.1 and 0.2. At constant R/L values, the average Nusselt number increases with increasing Rayleigh number because of the increase in the magnitude of the buoyancy forces. When the Rayleigh number is held constant, Nu increases with increasing R/L values, because of the increased heat transfer surface area. Furthermore, pure conduction heat transfer is increased with increasing absolute values of the vertical and/or horizontal eccentricities. At constant  $\epsilon_x$ , heat transfer is seen to be minimum, for conduction-dominated flows (Ra =  $10^3$  and  $10^4$ ), at  $\epsilon_v = 0$ . For convection-dominated flows (Ra =  $10^5$  and 10<sup>6</sup>), total heat transfer increases with increasing  $|\epsilon_v|$  for negative eccentricities, because of enhanced convection effects. For R/L = 0.1 and 0.2 and  $\epsilon_v > 0$ ,  $\overline{\text{Nu}}$ decreases and then increases for Ra =  $10^5$ , while it decreases for Ra =  $10^6$  as  $\epsilon_y$ increases. The presence of a positive  $\epsilon_y$  value for which heat transfer is minimum at Ra = 10<sup>5</sup> is due to the counteracting effects of increasing conduction and decreasing convection with increasing  $\epsilon_y$ . As  $\epsilon_y$  is increased, convection is decreased, while conduction is increased but at a lower rate. Further increase in  $\epsilon_{\nu}$ reverses the picture and  $\overline{Nu}$  increases again. For Ra =  $10^6$ , stratification effects being very high, the increase in conduction for  $\epsilon_v > 0$  does not offset the higher

Table 1. Average Nusselt number values

| Ra              | R/L = 0.1 |                  |                      |                     | R/L = 0.2      |                  |                     | R/L = 0.3           |       |                  |                     |
|-----------------|-----------|------------------|----------------------|---------------------|----------------|------------------|---------------------|---------------------|-------|------------------|---------------------|
|                 | •,        | $\epsilon_x = 0$ | $\epsilon_x = -0.15$ | $\epsilon_x = -0.3$ | ε <sub>y</sub> | $\epsilon_x = 0$ | $\epsilon_x = -0.1$ | $\epsilon_x = -0.2$ | €,    | $\epsilon_x = 0$ | $\epsilon_x = -0.1$ |
| 0               | - 0.3     | 5.501            | 5.616                | 6.365               | - 0.2          | -                | 8.273               | 9.549               | - 0.1 | 12.512           | 13.061              |
|                 | - 0.15    | 4.025            | 4.165                | 5.372               | -0.1           |                  | 6.933               | 8.283               |       |                  |                     |
|                 | 0         | 3.672            | 3.974                | 5.233               | 0              | 6.52             | 6.657               | 8.027               | 0     | 10.738           | 11.918              |
|                 | 0.15      | 4.025            | 4.165                | 5.372               | 0.1            |                  | 6.933               | 8.283               |       |                  |                     |
|                 | 0.3       | 5.501            | 5.616                | 6.365               | 0.2            |                  | 8.273               | 9.549               | 0.1   | 12.512           | 13.061              |
| 10 <sup>3</sup> | -0.3      |                  | 5.639                | 6.393               | -0.2           |                  | 8.279               | 9.554               | -0.1  |                  | 13.068              |
|                 | -0.15     |                  | 4.168                | 5.398               | -0.1           |                  | 6.934               | 8.29                |       |                  |                     |
|                 | 0         |                  | 3.981                | 5.243               | 0              |                  | 6.66                | 8.033               | 0     |                  | 11.92               |
|                 | 0.15      |                  | 4.167                | 5.397               | 0.1            |                  | 6.936               | 8.284               |       |                  |                     |
|                 | 0.3       |                  | 5.618                | 6.392               | 0.2            |                  | 8.274               | 9.552               | 0.1   |                  | 13.063              |
| 104             | -0.3      | 5.984            | 6.1                  | 6.764               | - 0.2          |                  | 8.776               | 10.137              | - 0.1 | 12.788           | 13.149              |
|                 | 0.15      | 4.605            | 4.741                | 5.876               | -0.1           |                  | 7.227               | 8.719               |       |                  |                     |
|                 | 0         | 4.142            | 4.425                | 5.703               | 0              | 6.662            | 6.835               | 8.354               | 0     | 11.652           | 11.967              |
|                 | 0.15      | 4.356            | 4.472                | 5.715               | 0.1            |                  | 7.097               | 8.575               |       |                  |                     |
|                 | 0.3       | 5.696            | 5.871                | 6.571               | 0.2            |                  | 8.448               | 9.83                | 0.1   | 12.584           | 13.11               |
| 10 <sup>5</sup> | -0.3      | 8.744            | 8.083                | 8.276               | - 0.2          |                  | 11.974              | 13.038              | -0.1  | 15.412           | 15.817              |
|                 | -0.15     | 7.914            | 7.435                | 7.702               | - 0.1          |                  | 10.606              | 11.811              |       |                  |                     |
|                 | 0         | 7.650            | 7.313                | 7.685               | 0              | 10.16            | 9.974               | 11.231              | 0     | 12.424           | 13.809              |
|                 | 0.15      | 7.222            | 6.811                | 7.339               | 0.1            |                  | 9.497               | 10.636              |       |                  |                     |
|                 | 0.3       | 7.356            | 6.986                | 7.473               | 0.2            |                  | 10.429              | 11.519              | 0.1   | 14.344           | 14.75               |
| 10 <sup>6</sup> | - 0.3     | 14.084           | 12.638               | 11.556              | - 0.2          |                  | 18.727              | 18.13               | -0.1  | 24.34            | 22.968              |
|                 | -0.15     | 12,943           | 12.453               | 11.486              | -0.1           |                  | 18.067              | 17.487              |       |                  |                     |
|                 | 0         | 12.214           | 12.183               | 11.425              | 0              | 18.748           | 17.602              | 17.203              | 0     | 23.24            | 21.379              |
|                 | 0.15      | 12.067           | 11.862               | 11.347              | 0.1            |                  | 16.742              | 16.766              |       |                  |                     |
|                 | 0.3       | 11.144           | 10.79                | 10.429              | 0.2            |                  | 16.344              | 16.076              | 0.1   | 23.82            | 21.134              |

decrease in convection and  $\overline{\text{Nu}}$  always decreases. For R/L=0.3, the above discussion still holds, but convection starts to dominate at Ra =  $10^6$ .

The effect of increasing  $|\epsilon_x|$  is to increase heat transfer for conduction-dominated flows, for the reasons stated above. At high Ra, total heat transfer values are dictated by the relative influence of convection and conduction in the wide and narrow gap regions. By increasing  $|\epsilon_x|$ , thermal convection by large recirculating vortices in the narrow gap region becomes more and more difficult, in contrast to the growing influence of the thermal conduction. At the same time, convection is increased in the wide gap region. However, this increase may not compensate for the decrease in heat transfer on the other side, even with the increased conduction there. This is in contrast to the case for which  $\epsilon_x = 0$ , where the available convective area is the same on both sides of the inner cylinder and convection is of equal importance. Depending on the relative effect of the abovementioned factors, heat transfer may decrease or increase with varying  $\epsilon_x$ . At the highest Rayleigh number considered, where convection is the dominant heat transfer mode, maximum heat transfer is obtained for  $\epsilon_x = 0$  and the total heat transfer decreases with increasing  $|\epsilon_x|$ .

#### **CONCLUDING REMARKS**

The NVF SCDS, presented in a companion article [1], was used to study the effect of eccentricity on natural convection in a horizontal annulus. At low Rayleigh numbers, total heat transfer was found to increase with increasing  $|\epsilon_y|$  and/or  $|\epsilon_x|$ . At high Rayleigh numbers, predictions revealed that heat transfer increases when moving the inner cylinder downward, decreases when moving it upward, and decreases when displacing it horizontally away from the vertical centerline of the enclosure.

#### REFERENCES

- 1. F. Moukalled and M. Darwish, New Bounded Skew Central Difference Scheme, Part 1: Formulation and Testing, *Numer. Heat Transfer*, *Part B*, vol. 31, pp. 91-110, 1997.
- 2. T. H. Kuehn and R. J. Goldstein, An Experimental and Theoretical Study of Natural Convection in the Annulus between Horizontal Concentric Cylinders, *J. Fluid Mech.*, vol. 74, pp. 695-709, 1976.
- J. R. Custer and E. J. Shaughnessy, Thermoconvective Motion of Low Prandtl Number Fluids within a Horizontal Cylindrical Annulus, J. Heat Transfer, vol. 99, pp. 596-602, 1977.
- 4. B. Farouk and S. I. Guceri, Laminar and Turbulent Natural Convection in the Annulus between Horizontal Concentric Cylinders, J. Heat Transfer, vol. 104, pp. 631-636, 1982.
- A. Castrejon and D. B. Spalding, An Experimental and Theoretical Study of Transient Free-Convection Flow between Horizontal Concentric Cylinders, Int. J. Heat Mass Transfer, vol. 31, no. 2, pp. 273-284, 1988.
- V. I. Bubnovich and P. M. Kolesnikov, Conjugate Unsteady-State Heat Transfer during Laminar Natural Convection in a Horizontal Annulus, J. Eng. Phys., vol. 51, no. 4, pp. 576-583, 1986.
- P. M. Kolesnikov and V. I. Bubnovich, Non-stationary Conjugate Free-Convective Heat Transfer in Horizontal Cylindrical Coaxial Channels, *Int. J. Heat Mass Transfer*, vol. 31, no. 6, pp. 1149-1156, 1988.
- 8. R. Kumar, Study of Natural Convection in Horizontal Annuli, Int. J. Heat Mass Transfer, vol. 31, no. 6, pp. 1137-1148, 1988.
- 9. S. B. Clemes, K. G. T. Hollands, and A. P. Brunger, Natural Convection Heat Transfer from Long Horizontal Isothermal Cylinders, *J. Heat Transfer*, vol. 116, pp. 96-104, 1994.
- C. H. Cho, K. S. Chang, and K. H. Park, Numerical Simulation of Natural Convection in Concentric and Eccentric Horizontal Cylindrical Annuli, J. Heat Transfer, vol. 104, pp. 624-630, 1982.
- 11. J. Prusa and L. S. Yao, Natural Convection Heat Transfer between Eccentric Horizontal Cylinders, J. Heat Transfer, vol. 105, pp. 108-116, 1983.
- 12. C. J. Ho and Y. H. Lin, Natural Convection Heat Transfer of Cold Water within an Eccentric Horizontal Cylindrical Annulus, *J. Heat Transfer*, vol. 110, pp. 894-900, 1988.
- 13. D. Naylor, H. M. Badr, and J. D. Tarasuk, Experimental and Numerical Study of Natural Convection between Two Eccentric Tubes, *Int. J. Heat Mass Transfer*, vol. 32, pp. 171-181, 1989.
- 14. E. M. Sparrow, P. C. Stryker, and M. A. Ansari, Natural Convection in Enclosures with Off-center Innerbodies, *Int. J. Heat Mass Transfer*, vol. 27, pp. 49-56, 1984.
- 15. M. Lacroix, Natural Convection Heat Transfer around Two Heated Horizontal Cylinders inside a Rectangular Cavity Cooled from Above, *Numer. Heat Transfer*, *Pan A*, vol. 21, pp. 37-54, 1992.

- C. J. Ho, W. S. Chang, and C. C. Wang, Natural Convection between Two Horizontal Cylinders in an Adiabatic Circular Enclosure, J. Heat Transfer, vol. 115, pp. 158-165, 1993.
- K. S. Chang, Y. H. Won, and C. H. Cho, Patterns of Natural Convection around a Square Cylinder in a Horizontal Circular Cylinder, J. Heat Transfer, vol. 105, pp. 273-280, 1983.
- P. H. Oosthuizen and J. T. Paul, Finite Element Study of Natural Convection Heat Transfer from a Prismatic Cylinder in an Enclosure, *Numer. Meth. Heat Transfer*, vol. 62, pp. 13-21, 1987.
- R. O. Warrington and R. E. Powe, The Transfer of Heat by Natural Convection between Bodies and Their Enclosures, Int. J. Heat Mass Transfer, vol. 28, no. 2, pp. 319-330, 1985.
- R. O. Warrington, P. K. Brown, and R. E. Powe, Natural Convection Heat Transfer within Enclosures at Reduced Pressures, *Proc. 8th Int. Heat Transfer Conf.*, vol. 4, pp. 1483-1488, 1986.
- 21. N. K. Ghaddar, Natural Convection Heat Transfer between a Uniformly Heated Cylindrical Element and Its Rectangular Enclosure, *Int. J. Heat Mass Transfer*, vol. 35, no. 10, pp. 2327-2334, 1992.
- 22. F. Moukalled and S. Acharya, Natural Convection in the Annulus between a Horizontal Circular Cylinder Placed Concentrically inside a Square Cylinder, *AIAA J. Thermophys. Heat Transfer*, vol. 10, pp. 524-531, 1996.
- 23. F. Moukalled and S. Acharya, Natural Convection in the Annulus between a Horizontal Circular Cylinder Placed Eccentrically inside a Square Cylinder, in review.
- 24. M. J. Cho and M. K. Chung, New Treatment of Nonorthogonal Terms in the Pressure-Correction Equation, *Numer. Heat Transfer*, *Part B*, vol. 26, pp. 133-145, 1994.
- 25. P. D. Thomas and J. F. Middlecoff, Direct Control of the Grid Point Distribution in Meshes Generated by Elliptic Equations, AIAA J., vol. 18, no. 6, pp. 652-656, 1980.
- S. V. Patankar, C. H. Liu, and E. M. Sparrow, Fully Developed Flow and Heat Transfer in Ducts Having Streamwise-Periodic Variations of Cross-Sectional Area, J. Heat Transfer, vol. 99, pp. 180-186, 1977.